A Flexible, Moment-Preserving and Monotone Discretization of the Multidimensional Angular Fokker-Planck Operator

Charles Bienvenue,[*,a] Ahmed Naceur,[a] Jean-François Carrier,[b] and Alain Hébert[a]

[a] *Institut de génie nucleaire, Polytechnique Montréal, Montréal, H3C 3A7, Canada*

[b] *Département de physique, Université de Montréal, Montréal, H3T 1J4, Canada*

[*]Email: charles.bienvenue@polymtl.ca

Number of pages: 32
Number of tables: 0
Number of figures: 7

Abstract

A monotone finite-difference scheme is proposed for the multidimensional angular Fokker-Planck operator in discrete ordinates calculations. It is compatible with nonorthogonal quadrature sets on the unit sphere and preserves the null space, the zeroth and the first three angular moments of the analytical angular Fokker-Planck operator. Numerical results demonstrate that this discretization, combined with the suitable Galerkin quadrature method, eliminates spurious oscillations in the flux solution related to highly anisotropic scattering.

Keywords — Transport Equation, Discrete Ordinates, Fokker-Planck Operator, Finite-difference schemes

I. INTRODUCTION

Angular discretization of the transport equation by the discrete ordinates (S_N) method leads to numerical issues. In presence of highly forward-peaked scattering, the S_N method can produce highly inaccurate solutions, but with Gauss-Legendre quadrature in 1D geometry [1]. Pautz and Adams have shown that the source iteration process can even diverge, notably in scattering-dominated medium [2]. Such divergence is due to inappropriate angular discretization approximations, which can introduce a non-physical multiplication factor in the medium, leading to an absence of a steady-state solution. The Galerkin quadrature methodology has been developed to tackle these issues and to make the S_N method robust [1, 3]. However, the Galerkin method does not provide a monotone representation of the angular flux scattering [4, 5]. Undesirable numerical artifacts still can appear in the solution, such as rather important oscillations in the presence of anisotropic scattering, distinct from the well-known ray effects in multidimensional transport [6].

The purpose of this paper is to propose a methodology to mitigate these monotonicity issues related to highly anisotropic scattering using the angular Fokker-Planck (AFP) operator. Following the work of Landesman and Morel, the forward-peaked elastic scattering handling can be transferred from the Boltzmann operator to the AFP operator, for which monotone and moment-preserving finite-difference schemes exits [7]. For the 1D AFP operator, the finite-difference scheme from Morel [8], applicable to any choice of quadrature, is used. For the multidimensional AFP operator, a finite-difference scheme is developed based on the Voronoi tessellation of the unit sphere [9]. This scheme is a generalization of the previous work of Morel *et al.* [10] with product quadrature sets to nonorthogonal quadrature sets on the unit sphere.

This paper is organized as follows. In Sect. II, we describe the Boltzmann Fokker-Planck equation, which contains the ingredients of the angular discretization proposed in this work. In Sect. III, the discrete ordinates and Galerkin quadrature methods formalism are introduced. In Sect. IV, finite-difference schemes for the Fokker-Planck operator are developed to be compatible with nonorthogonal quadrature sets. Finally, in Sect. V, impacts of the proposed methodology for angular discretization on energy deposition benchmarks are presented and discussed.

II. THE BOLTZMANN FOKKER-PLANCK EQUATION

The presented angular discretization is based on the Boltzmann Fokker-Planck (BFP) equation, which consists of the linear Boltzmann transport equation to which Fokker-Planck (FP) terms are added. Przybylski and Ligou have introduced it to deal accurately with both small and large energy-loss interactions by having specific treatment for each of them [11]. The main idea is that interactions leading to small energy losses and angular deflection, called soft interactions, are handled by the FP operator, while interactions leading to large energy transfer, called catastrophic interactions, are handled by the Boltzmann operator. The FP operator is an asymptotic limit of the Boltzmann operator for small energy loss and direction change [12].

Let $\mathbb{S}^2 = \left\{\mathbf{\Omega} = (\mu, \eta, \xi) \in \mathbb{R}^3 : ||\mathbf{\Omega}|| = 1\right\}$ be the unit sphere, $\mathbf{\Omega}$, the particle direction, and $\mu, \eta, \xi \in [-1, 1]$ are direction cosines along $x-$, $y-$ and $z-$axis, respectively. Let E, the particle energy and $\mathbf{r} = (x, y, z) \in \mathbb{R}^3$, the particle position. The steady-state BFP equation is given by

$$\mathbf{\Omega} \cdot \nabla \Psi(\mathbf{r}, \mathbf{\Omega}, E) + \Sigma_t(\mathbf{r}, E)\Psi(\mathbf{r}, \mathbf{\Omega}, E) = Q^{\texttt{FP}}(\mathbf{r}, \mathbf{\Omega}, E) + Q^{\texttt{B}}(\mathbf{r}, \mathbf{\Omega}, E) + Q^{\texttt{ext}}(\mathbf{r}, \mathbf{\Omega}, E)\,, \tag{1}$$

where $Q^{\texttt{ext}}(\mathbf{r}, \mathbf{\Omega}, E)$ consists of fixed external sources of particles. The Fokker-Planck operator, with respectively the continuous slowing-down (CSD) and angular Fokker-Planck (AFP) terms, is given by [13]

$$Q^{\texttt{FP}}(\mathbf{r}, \mathbf{\Omega}, E) = Q^{\texttt{CSD}}(\mathbf{r}, \mathbf{\Omega}, E) + Q^{\texttt{AFP}}(\mathbf{r}, \mathbf{\Omega}, E)\,, \tag{2}$$

with

$$Q^{\texttt{CSD}}(\mathbf{r}, \mathbf{\Omega}, E) = \frac{\partial}{\partial E}\left[S(\mathbf{r}, E)\Psi(\mathbf{r}, \mathbf{\Omega}, E)\right] \quad \text{and} \quad Q^{\texttt{AFP}}(\mathbf{r}, \mathbf{\Omega}, E) = T(\mathbf{r}, E)\nabla^2_{\Omega}\Psi(\mathbf{r}, \mathbf{\Omega}, E)\,. \tag{3}$$

The Boltzmann operator, in which scattering cross-sections are expanded in Legendre polynomials and angular flux are expanded in N_p spherical harmonics, is [14]

$$Q^{\texttt{B}}(\mathbf{r}, \mathbf{\Omega}, E) = \int_0^{\infty} dE' \sum_{p=1}^{N_p} \frac{2\ell_p + 1}{4\pi} \Sigma_{s,\ell_p}(\mathbf{r}, E' \to E) R_{\ell_p}^{m_p}(\mathbf{\Omega}) \Phi_p(\mathbf{r}, E')\,, \tag{4}$$

with the angular flux moments

$$\Phi_p(\mathbf{r}, E') = \int_{\mathbb{S}^2} d^2\Omega' R_{\ell_p}^{m_p}(\mathbf{\Omega}')\Psi(\mathbf{r}, \mathbf{\Omega}', E')\,, \tag{5}$$

where $R_\ell^m(\mathbf{\Omega})$ is the real spherical harmonics, as defined in Hébert [14] using Ferrer definitions of the associated Legendre polynomials, $\Psi(\mathbf{r}, \mathbf{\Omega}, E)$ is the angular flux, $\Sigma_t(\mathbf{r}, E)$ is the macroscopic total cross-section, $\Sigma_{s,\ell}(\mathbf{r}, E' \to E)$ is the ℓ-order Legendre moment of the macroscopic scattering cross-section from energies E' to E, $S(\mathbf{r}, E)$ is the soft stopping power and $T(\mathbf{r}, E)$ is the soft momentum transfer. For a more formal definition of the cross-sections, stopping powers and momentum transfer in the BFP, as well as the definition of the soft and catastrophic interactions, see [15, 16]. The indexes ℓ_p and m_p are functions of their index p, whose values are given following a Gramm-Schmidt process to select a subset of spherical harmonics, as described in Sect. III.

The multigroup discretization of this equation, which divides the energy domain into G energy groups, and the discretization schemes for both streaming (spatial derivative) and CSD terms (energy derivative), are described in previous works [4, 11, 15, 17, 18, 19] and are not the focus of this paper. This paper aims to propose a flexible angular discretization framework that capitalizes on the capacities of the BFP equation, based on its AFP and Boltzmann operators. Note that, while the CSD term is employed in this work for electron transport, the presented method does not rely on it. The following schemes could equally be applied to the Boltzmann equation by including the AFP operator in it and can be equally be applied to neutral particle transport. Particularly, it could be of interest for very fast neutron transport using discrete ordinates solvers [20].

The elastic scattering cross-sections can be decomposed into soft and catastrophic components [7]. Let's assume a material identified by index i. Let L be the order of the cross-sections Legendre expansion and $\Sigma_{s,\ell,i}^{g\to g}$ be the ℓ-order Legendre moment of the elastic scattering cross-section in group g in material i. Let $L_{\texttt{max}} \leq L$ be the last non-zero Legendre moments of the scattering in group g in material i (these indices are omitted for simplicity). The Legendre moments of the soft are assumed to be given by

$$\Sigma_{s,\ell,i}^{g\to g,\texttt{soft}} = \Sigma_{s,0,i}^{g\to g,\texttt{soft}} - T_{g,i}\ell(\ell+1) \tag{6}$$

for $\ell \in \{1, ..., L_{\texttt{max}}\}$. This expression is obtained by establishing equality between the eigenvalues of the Boltzmann and the AFP operator applied to the Legendre polynomials [13]. This method sets a relation, which depends on two undefined parameters $\Sigma_{s,0,i}^{g\to g,\texttt{soft}}$ and $T_{g,i}$, such as moments of the Boltzmann operator are preserved by the Fokker-Planck operator. Landesman and Morel proposed to equate $\Sigma_{s,L_{\texttt{max}}-1,i}^{g\to g,\texttt{soft}} = \Sigma_{s,L_{\texttt{max}}-1,i}^{g\to g}$ and $\Sigma_{s,L_{\texttt{max}},i}^{g\to g,\texttt{soft}} = \Sigma_{s,L_{\texttt{max}},i}^{g\to g}$ to define these parameters, which results in

$$T_{g,i} = \frac{\Sigma_{s,L_{\texttt{max}}-1,i}^{g\to g} - \Sigma_{s,L_{\texttt{max}},i}^{g\to g}}{2L_{\texttt{max}}}\,, \tag{7}$$

and

$$\Sigma_{s,0,i}^{g\to g,\texttt{soft}} = \Sigma_{s,L_{\texttt{max}},i}^{g\to g} + T_{g,i}L_{\texttt{max}}(L_{\texttt{max}}+1)\,. \tag{8}$$

The soft component of the elastic cross-sections should then be withdrawn from cross-sections since the AFP operator, jointly with the momentum transfer given by Eq. 7, is used to treat that soft scattering. The resulting catastrophic cross-sections are given by

$$\Sigma_{s,\ell,i}^{g\to g,\texttt{catas}} = \Sigma_{s,\ell,i}^{g\to g} - \Sigma_{s,\ell,i}^{g\to g,\texttt{soft}}\,. \tag{9}$$

The Legendre moments of the cross-sections are obtained by substituting Eq. 8 and Eq. 6 into Eq. 9. Thus, the total elastic cross-sections are redefined as

$$\Sigma_{t,g,i}^{\texttt{catas}} = \Sigma_{t,g,i} - \Sigma_{s,L_{\texttt{max}},i}^{g\to g} - T_{g,i}L_{\texttt{max}}(L_{\texttt{max}}+1)\,, \tag{10}$$

and the ℓ-order Legendre moment of the scattering cross-sections are redefined as

$$\Sigma_{s,\ell,i}^{g\to g,\texttt{catas}} = \Sigma_{s,\ell,i}^{g\to g} - \Sigma_{s,L_{\texttt{max}},i}^{g\to g} - T_{g,i}\left[L_{\texttt{max}}(L_{\texttt{max}}+1) - \ell(\ell+1)\right]\,. \tag{11}$$

This method, as presented, includes the extended transport correction [21, 22]. The goal of this operation is to transfer the handling of forward-peaked scattering from the Boltzmann operator, which encounters monotonicity issues with such scattering [4], to the Fokker-Planck operator, which can be tackled by finite-difference discretization schemes [8, 10].

III. DISCRETE ORDINATES METHOD AND GALERKIN QUADRATURE

The discrete ordinates method, also known as the $\mathrm{S_N}$ method, consists in the discretization of the angular domain, the unit sphere $\mathbb{S}^2$, in N_d discrete directions $\mathbf{\Omega}_n$ for $n = \{1, ..., N_d\}$. Numerical quadrature is used to deal with integrals over $\mathbb{S}^2$ using weights w_n associated with each direction $\mathbf{\Omega}_n$. The S_N equations are obtained by requiring the one-speed transport equation in group g to hold when evaluated at each $\mathbf{\Omega}_n$ such as

$$\mathbf{\Omega}_n \cdot \nabla \Psi_{g,n}(\mathbf{r}) + \Sigma_{t,g} \Psi_{g,n}(\mathbf{r}) = Q^{\mathtt{CSD}}_{g,n}(\mathbf{r}) + Q^{\mathtt{AFP}}_{g,n}(\mathbf{r}) + Q^{\mathtt{B}}_{g,n}(\mathbf{r}) + Q^{\mathtt{ext}}_{g,n}(\mathbf{r}) \,, \tag{12}$$

where the Boltzmann operator is given by

$$Q^{\mathtt{B}}_{g,n}(\mathbf{r}) = \sum_{g'=1}^{G} \sum_{p=1}^{N_p} \frac{2\ell_p + 1}{4\pi} \Sigma^{g' \to g}_{s,\ell_p}(\mathbf{r}) R^{m_p}_{\ell_p}(\mathbf{\Omega}_n) \Phi_{g',p}(\mathbf{r}) \,, \tag{13}$$

with g' and g being the energy group of the incoming and outgoing particle, and where

$$\Phi_{g',p}(\mathbf{r}) = \sum_{n=1}^{N_d} \omega_n R^{m_p}_{\ell_p}(\mathbf{\Omega}_n) \Psi_{g',n}(\mathbf{r}) \,. \tag{14}$$

The AFP operator discretization will be given in Sect. IV. The CSD operator discretization will not be discussed here, since it is independent of the proposed angular discretization, see [17, 11, 18] for a detailed treatment of that operator. The S_N method leads to a set of N_d equations that can be solved using iterative techniques. At each iteration, along each direction, the flux solution is computed across the spatial domain, in a process often referred to as sweeping [14], using the most up-to-date particle sources. Then, sources are actualized using the last estimation of the flux solution. To achieve this, the N_d discrete angular fluxes in $\mathbf{\Psi}_g = (\Psi_{g,1}, \Psi_{g,2}, ..., \Psi_{g,N_d})$ have to be converted in N_p spherical harmonics flux moments in $\mathbf{\Phi}_g = \left(\Phi_{g,1}, \Phi_{g,2}, ..., \Phi_{g,N_p}\right)$. The resulting spherical harmonics flux moments are multiplied by their corresponding Legendre moments of the scattering cross-section to obtain the Legendre moments of the Boltzmann, which are then converted back into discrete angular sources for the following iteration. These conversion operations can be expressed in matrix form using both the discrete-to-moment ($\mathbf{D}$) and the moment-to-discrete

($\mathbf{M}$) matrices such as

$$\mathbf{\Phi}_g = \mathbf{D}\mathbf{\Psi}_g \quad \text{and} \quad \mathbf{\Psi}_g = \mathbf{M}\mathbf{\Phi}_g \,. \tag{15}$$

The standard discrete ordinates conversion matrix components are given by

$$D_{p,n} = w_n R_{\ell_p}^{m_p}(\mathbf{\Omega}_n) \quad \text{and} \quad M_{n,p} = \frac{2\ell_p + 1}{4\pi} R_{\ell_p}^{m_p}(\mathbf{\Omega}_n) \,, \tag{16}$$

for $n = 1, N_d$ and $p = 1, N_p$. In 1D Cartesian geometry, these conversion matrices components can be reduced to

$$D_{p,n} = w_n P_{\ell_p}(\mu_n) \quad \text{and} \quad M_{n,p} = \frac{2\ell_p + 1}{2} P_{\ell_p}(\mu_n) \,, \tag{17}$$

where $P_{\ell_p}(\mu_n)$ are Legendre polynomials and $\ell_p = p - 1$. The quadrature on the unit sphere reduces to a quadrature over the direction cosine μ domain, which spans from -1 to 1. With these matrices, the vector containing the N_d Boltzmann sources, $\mathbf{Q}_g^{\mathtt{B}} = \left(Q_{g,1}^{\mathtt{B}}, Q_{g,2}^{\mathtt{B}}, ..., Q_{g,N_d}^{\mathtt{B}}\right)$, is given by

$$\mathbf{Q}_g^{\mathtt{B}} = \sum_{g'=1}^{G} \mathbf{M}\mathbf{\Sigma}^{g' \to g}\mathbf{D}\mathbf{\Psi}_{g'} \,, \tag{18}$$

where $\mathbf{\Sigma}^{g' \to g}$ is a $N_p \times N_p$ diagonal matrix with each component associated with ℓ_p-order Legendre moments of the scattering cross-section ($\mathbf{\Sigma}_{p,p}^{g' \to g} = \Sigma_{s,\ell_p}^{g' \to g}$). The definition of indexes ℓ_p and m_p depending on index p can seem messy, but it is a compact and versatile notation that enables any choice of a subset of spherical harmonics. For instance, based on Reed's S_2 suitable interpolation basis for level-symmetric quadrature in 2D Cartesian geometry [23], composed of R_0^0, R_1^0, R_1^1 and R_2^1, the corresponding indexes are given by $\boldsymbol{\ell} = (0, 1, 1, 2)$ and $\mathbf{m} = (0, 0, 1, 1)$, and the diagonal of the $\mathbf{\Sigma}^{g' \to g}$ matrix is given by $(\Sigma_{s,0}^{g' \to g}, \Sigma_{s,1}^{g' \to g}, \Sigma_{s,1}^{g' \to g}, \Sigma_{s,2}^{g' \to g})$.

It is well known that there is an equivalence in 1D Cartesian or spherical geometry between the discrete ordinates solution, using N-order Gauss-Legendre quadrature with Legendre expansion of degree $N-1$, and the $(N-1)$-order spherical harmonics (or P_N) solution using Mark boundary conditions [14, 13]. In fact, with such quadrature and Legendre expansion, both conversion matrices $\mathbf{M}$ and $\mathbf{D}$ are square and inverse of each other, which is very desirable since it ensures accurate integration regardless of the strength of the anisotropy [4]. It ensures an exact integration of a Dirac scattering and that the commonly used transport correction leaves the solution of the transport equation invariant, which is not the case with any other quadrature choice [1]. This is

a major shortcoming in multidimensional geometries since there is no known quadrature on the unit sphere or choice of polynomial basis that results naturally to conversion matrices which are inverse of each other. While the classical S_N method can lead to inaccurate and non-physical solutions, it also can prevent convergence by allowing a scattering ratio to exceed one, which mostly happens in scattering-dominated mediums [2]. Such a scattering ratio is associated with each scattering moment, and a single discrepancy is sufficient to disrupt the iterative process. These problems become apparent when dealing with charged particles, for which scattering is dominant and scattering is highly forward-peaked.

The Galerkin quadrature method, developed by Morel, solves the most important issues of the classical S_N method [1, 3]. It ensures the exact integration of a Dirac scattering and, corollary, that the transport correction leaves the solution of the transport equation invariant [4]. It guarantees that the scattering ratios remain below one for all moments, thereby ensuring proper convergence of the source iteration process [2]. The Galerkin method, however, does not offer a solution to artifacts related to scattering positivity [1]. A Galerkin quadrature is obtained by inverting either the discrete-to-moment or the moment-to-discrete matrix, evaluated using Eqs. 16 or 17, i.e.

$$\mathbf{D} = \mathbf{M}^{-1} \,. \tag{19}$$

This requires that $\mathbf{D}$ and $\mathbf{M}$ are square and invertible matrices. If we can compute $\mathbf{M}$ with these two properties, it can be inverted to find $\mathbf{D}$, or vice-versa, to obtain a Galerkin quadrature [1, 3, 24]. For these matrices to be square, the number of directions N_d (nodes of the quadrature) has to be strictly equal to the number of basis functions used in the angular flux expansion. To be invertible, linearly independent matrix columns are required, which is not the case for every choice of basis functions. While it is not part of the present work, the reader should also be aware that Shands *et al.* [3] have developed a new Galerkin quadrature method that eliminate the need for matrix inversion.

For 1D Cartesian geometries, Legendre polynomials can be used as basis functions. For a quadrature with N_d nodes, the Legendre polynomials up to order $N_d - 1$ should be chosen as the basis function of the angular flux expansion. The discrete-to-moment matrix ($\mathbf{D}$) can then be computed using Eqs. 17, and it can be inverted to obtain the moment-to-discrete matrix ($\mathbf{M}$), or vice-versa, without any additional difficulties. This is because the previously stated choice of

Legendre polynomials yields square and invertible matrices. The Gauss-Legendre quadrature is the sole quadrature choice that naturally produces a Galerkin quadrature with classical S_N [13]. The Galerkin quadrature method allows the use of Gauss-Lobatto quadrature, which is very useful when dealing with normally incident particle sources, due to its two nodes aligned with the Cartesian reference system axis ($\mu = -1$ and $\mu = 1$) [4].

For multidimensional geometries, the real spherical harmonics are used as basis functions. For a quadrature set with N_d nodes, a subset of spherical harmonics has to be chosen knowing that not every subset leads to an invertible discrete-to-moment matrix (or vice-versa). While rules for suitable subset of spherical harmonics exist for some quadrature sets [1, 3, 25], a Gram-Schmidt procedure is proposed by Drumm *et al.* to choose a subset of spherical harmonics such as the columns of $\mathbf{D}$ (or $\mathbf{M}$) are linearly independent, regardless of the choice of quadrature [26, 27]. This procedure, which is described in Alg. 1, is employed in this work. It should be noted that quadrature on the unit sphere and real spherical harmonics basis functions can also be used in 1D geometry.

The efficiency of a quadrature set defined over the unit sphere with N_d nodes that integrate a subspace of spherical harmonics of maximum degree N is given by [28]

$$\eta = \frac{(N+1)^2}{3N_d} \,. \tag{20}$$

A quadrature set is considered optimal if $\eta \approx 1$, and suboptimal if $\eta < 1$. An optimal quadrature set is desirable in S_N transport calculations because the multiplication of nodes increases the number of required sweeps over the spatial domain per iteration to achieve a specific accuracy. The most straightforward quadrature over the sphere is a product quadrature, which consists of the product of two quadrature sets over a line segment, along the μ and ϕ coordinates. This quadrature with $N_d = 2N^2$ nodes divides the angular domain in orthogonal meshes. However, accurate calculations with such a quadrature set are exceedingly expensive because the quadrature efficiency is constrained between $\eta = 1/6$ ($N \to \infty$) and $\eta = 3/8$ ($N = 2$), as shown in Fig. 2. The node distribution over the sphere is far from uniform with dense pileups of nodes near $\mu = \pm 1$ while it also lacks 4-fold ($\mathbf{C}_4$) rotational symmetry around the three axes, as it can be seen in Fig. 1. To deal with these issues, the so-called level-symmetric quadrature sets were developed. For example, Carlson's ES_N quadrature [29], which presents a more uniform node distribution and $\mathbf{C}_4$

Algorithm 1 Gram-Schmidt procedure for selecting a suitable subset of spherical harmonics to ensure invertibility of the discrete-to-moment ($\mathbf{D}$) or the moment-to-discrete ($\mathbf{M}$) matrices, considering machine precision (ϵ) and geometry dimension (N_{dim}).

$(\boldsymbol{\ell}[1], \mathbf{m}[1]) \leftarrow (0, 0)$
for $\ell \in \{1, ..., N_d\}$ **do**
  $\mathbf{D}[1, n] \leftarrow \omega_n R_0^0(\boldsymbol{\Omega}_n)$ or $\mathbf{M}[n, 1] \leftarrow \frac{1}{4\pi} R_0^0(\boldsymbol{\Omega}_n)$
  $\mathbf{v}_1[n] \leftarrow R_0^0(\boldsymbol{\Omega}_n)$
  $\mathbf{u}_1[n] \leftarrow \mathbf{v}_1[n] / \|\mathbf{v}_1\|$
end for
$i \leftarrow 1$
for $\ell \in \{1, ..., L_{\texttt{max}}\}$ **do**
  if $N_{\text{dim}} = 2$ **then** $m_{\min} = 0$ **else if** $N_{\text{dim}} = 3$ **then** $m_{\min} = -\ell$ **end if**
  for $m \in \{m_{\min}, ..., \ell\}$ **do**
    for $\ell \in \{1, ..., N_d\}$ **do**
      $\mathbf{v}_{i+1}[n] \leftarrow R_\ell^m(\boldsymbol{\Omega}_n)$
    end for
    $\mathbf{v}_{i+1} \leftarrow \mathbf{v}_{i+1} - \sum_{n=1}^{i} \langle \mathbf{u}_n, \mathbf{v}_{i+1} \rangle \mathbf{u}_\mathbf{n}$
    if $\|\mathbf{v}_{i+1}\| > \epsilon$ **then**
      $(\boldsymbol{\ell}[i+1], \mathbf{m}[i+1]) \leftarrow (\ell, m)$
      for $\ell \in \{1, ..., N_d\}$ **do**
        $\mathbf{D}[i+1, n] = \omega_n R_\ell^m(\boldsymbol{\Omega}_n)$ or $\mathbf{M}[n, i+1] \leftarrow \frac{2\ell+1}{4\pi} R_\ell^m(\boldsymbol{\Omega}_n)$
        $\mathbf{u}_{i+1}[n] = \mathbf{v}_{i+1}[n] / \|\mathbf{v}_{i+1}\|$
      end for
      $i \leftarrow i + 1$
    end if
    if $i = N_d$ **then return** ($\mathbf{D}$ or $\mathbf{M}$, $\boldsymbol{\ell}$ and $\mathbf{m}$) **end if**
  end for
end for

rotational symmetry around the axis. It has $N_d = N(N+2)$ nodes and the resulting efficiency of this kind of quadrature still is constrained between $\eta = 1/3$ ($N \to \infty$) and $\eta = 3/8$ ($N = 2$). Optimal, or sightly optimal, quadrature sets do exist, such as the ones of Lebedev [30, 31, 32]. Lebedev quadrature possesses octahedral rotation symmetry with inversion and has, as the Gauss-Lobatto in 1D, nodes along the Cartesian reference system axis [30]. While these nodes along the axis are useful to treat normally incident beams, they lead to an asymmetric subset of spherical harmonics for the Galerkin quadrature methods, which is not ideal (see [25], p.141).

IV. FINITE-DIFFERENCE SCHEMES FOR THE ANGULAR FOKKER-PLANCK TERM

Extracting the momentum transfer term from the cross-sections to treat the elastic forward-peaked scattering with the AFP operator rather than the Boltzmann operator allows the use of

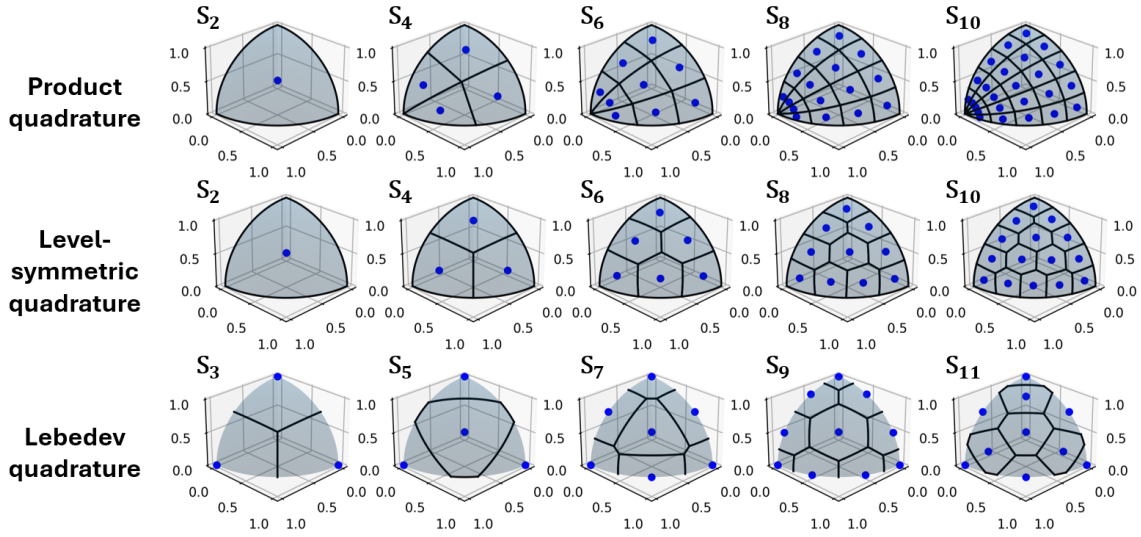

Fig. 1. Voronoi tessellation of the unit sphere positive octant based on the nodes (in blue) of product quadrature (Gauss-Legendre quadrature along μ and Chebychev quadrature along ϕ), level-symmetric quadrature (Carlson ES_N quadrature) and Lebedev quadrature.

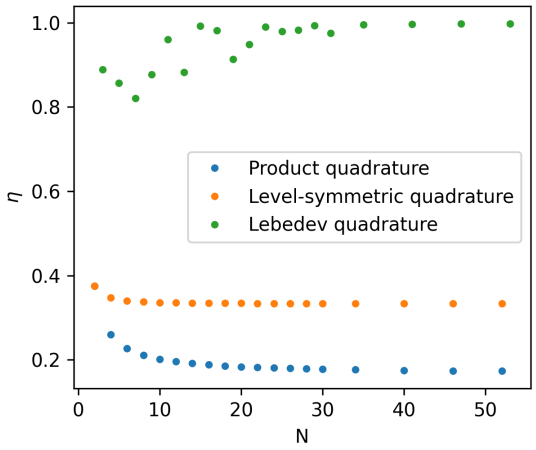

Fig. 2. Quadrature efficiency of the product quadrature (Gauss-Legendre quadrature along μ and Chebychev quadrature along ϕ), the level-symmetric quadrature (Carlson ES_N quadrature) and Lebedev quadrature.

finite-difference schemes to enforce the positivity and monotonicity of the forward-peaked scattering. The N_d FP angular sources are given by

$$\mathbf{Q}_g^{\texttt{AFP}} = T_g \mathcal{M} \mathbf{\Psi}_g \,, \tag{21}$$

where T_g is the momentum transfer defined in Sect. II and the square $N_d \times N_d$ mapping matrix $\mathcal{M}$ define the FP scattering between N_d angular flux. It is worth noting that, unlike T_g, $\mathcal{M}$ is independent of energy and position, unlike T_g, and therefore needs to be computed only once before the iterative process. Leaving the forward-peaked part of the elastic scattering in the cross-sections is equivalent to extracting the momentum transfer from cross-sections and computing the AFP source using the following mapping matrix [5, 7]

$$\mathcal{M} = \mathbf{M}\mathbf{\Sigma}^{\texttt{AFP}}\mathbf{D}\,, \quad \text{with} \quad \mathbf{\Sigma}^{\texttt{AFP}}_{n,p} = \begin{cases} -\ell_p(\ell_p+1) & \text{if} \quad n = p \\ 0 & \text{otherwise} \end{cases}\,, \tag{22}$$

where $\mathbf{M} = \mathbf{D}^{-1}$, based on the Galerkin quadrature method. It will be referred to as the Galerkin scheme. It preserves the moments of the angular Fokker-Planck operator with the selected subset of spherical harmonics, but it does not yield a monotone mapping matrix $\mathcal{M}$ as the following finite-difference scheme.

IV.A. Finite-difference scheme for the 1D angular Fokker-Planck operator

Morel has developed a finite-difference scheme for the 1D AFP operator that preserves both the zeroth and first angular moments of the analytical AFP operator [8, 7]. The resulting mapping matrix is a tridiagonal matrix in which components are given by

$$\mathcal{M}_{n,m} = \begin{cases} -C_n & \text{if } n = m \\ C_n^- & \text{if } n = m+1 \\ C_n^+ & \text{if } n = m-1 \\ 0 & \text{otherwise} \end{cases} \tag{23}$$

where the terms are defined by

$$C_n^- = \frac{C_{n-1/2}}{w_n(\mu_n - \mu_{n-1})}, \quad C_n^+ = \frac{C_{n+1/2}}{w_n(\mu_{n+1} - \mu_n)} \quad \text{and} \quad C_n = C_n^- + C_n^+ \,, \tag{24}$$

with the recursion formula

$$C_{n+1/2} = C_{n-1/2} - 2\mu_n w_n \quad \text{and} \quad C_{1/2} = 0 \,. \tag{25}$$

The matrix $\mathcal{M}$ is negative semidefinite (real eigenvalues less or equal to zero) and monotone (negative diagonal and positive off-diagonal elements). This discretization scheme can be described as positive since it will yield positive FP angular sources given positive angular flux [8, 4]. This scheme is compatible with any choice of quadrature set.

IV.B. Finite-difference scheme for the multidimensional angular Fokker-Planck operator

Morel *et al.* have extended the 1D finite-difference FP scheme to multidimensional geometries [10, 4]. The proposed scheme is however constrained to product quadrature, generating angular mesh boundaries that are aligned with director cosine μ and azimuthal angle ϕ. When the product quadrature is constructed with the Chebychev azimuthal quadrature, it enforces the preservation of the zeroth and the three first angular moments of the AFP operator. The resulting mapping matrix $\mathcal{M}$ components, over 2D and 3D quadrature, are given in Appendix A. It is negative semidefinite, it is monotone and it yields positive sources. However, as underlined in the previous section, product quadrature sets are far from optimal quadrature ones, their nodes are unevenly distributed on the sphere and they lack $\mathbf{C}_4$ rotational symmetry around the axes. Using such quadrature in transport calculations is extremely inefficient due to the enormous amount of nodes $\mathbf{\Omega}_n$ required to achieve a specific level of angular accuracy, which involves sweeping over the spatial domain for each of these directions. To tackle these shortcomings, we have extended the approach to nonorthogonal quadrature on the unit sphere.

The AFP operator, $Q_g^{\mathtt{AFP}}(\mathbf{\Omega})$, is given by [9, 33]

$$Q_g^{\mathtt{AFP}}(\mathbf{\Omega}) = T_g \nabla_\Omega^2 \Psi_g(\mathbf{\Omega}) = T_g \nabla_t \cdot \nabla_t \Psi_g(\mathbf{\Omega}) \,, \tag{26}$$

where ∇^2 is the Laplace operator and ∇_t is the tangential gradient on the unit sphere $\mathbb{S}^2$ given by

$$\nabla_t \Psi_g(\mathbf{\Omega}) = \nabla \Psi_g(\mathbf{\Omega}) - [\nabla \Psi_g(\mathbf{\Omega}) \cdot \mathbf{n}(\mathbf{\Omega})]\, \mathbf{n}(\mathbf{\Omega})\,, \tag{27}$$

where ∇ is the usual gradient in $\mathbb{R}^3$ and $\mathbf{n}(\mathbf{\Omega})$ is the unit normal vector on $\mathbb{S}^2$ at $\mathbf{\Omega}$. The integration of the AFP operator over the unit sphere (leftmost expression in Eq. 28) can be described either as the sum of the integral over N_d non-overlapping regions $\mathbf{\Omega}_n$ covering the totality of $\mathbb{S}^2$ (middle expression in Eq. 28) or by numerical quadrature on $\mathbb{S}^2$ (rightmost expression in Eq. 28), such as

$$\int_{\mathbb{S}^2} d^2\Omega Q_g^{\texttt{AFP}}(\mathbf{\Omega}) = \sum_{n=1}^{N_d} \int_{\mathbf{\Omega}_n} d^2\Omega Q_g^{\texttt{AFP}}(\mathbf{\Omega}) = \sum_{n=1}^{N_d} \omega_n Q_{g,n}^{\texttt{AFP}}\,, \tag{28}$$

where ω_n are the quadrature weights and $Q_{g,n}^{\texttt{AFP}}$ the discretized AFP operator. An example of such N_d non-overlapping regions over $\mathbb{S}^2$ is given in Fig. 3. This discretized operator can be deduced by association from the previous equation and integral over region $\mathbf{\Omega}_n$ can be simplified using divergence theorem over the spherical domain [33, 34],

$$Q_{g,n}^{\texttt{AFP}} = \frac{1}{\omega_n} \int_{\mathbf{\Omega}_n} d^2\Omega Q_g^{\texttt{AFP}}(\mathbf{\Omega}) = \frac{T_g}{\omega_n} \oint_{\delta\mathbf{\Omega}_n} d\ell \nabla_t \Psi_g(\mathbf{\Omega}) \cdot \mathbf{n}_\ell\,, \tag{29}$$

where $\delta\mathbf{\Omega}_n$ is the boundary of the region $\mathbf{\Omega}_n$ and $\mathbf{n}_\ell$ is the normal vector at region boundary on $\mathbb{S}^2$. Assuming that the region $\mathbf{\Omega}_n$ is a polygon with J_n sides, then the integral can be rewritten as the sum of the J_n integrals over the edges of the n^{th} region,

$$Q_{g,n}^{\texttt{AFP}} = \frac{T_g}{\omega_n} \sum_{j=1}^{J_n} \int_{\delta\Omega_{n,j}} d\ell \nabla_t \Psi_g(\mathbf{\Omega}) \cdot \mathbf{n}_\ell\,. \tag{30}$$

The central finite-difference is used to approximate the derivative on each edge of the polygon and this derivate is assumed to be constant over the entire edge. The previous expression can be approximated by

$$Q_{g,n}^{\texttt{AFP}} = \frac{T_g}{\omega_n} \sum_{j=1}^{J_n} \ell_{n,j} \left[\frac{\Psi_{g,m_{n,j}} - \Psi_{g,n}}{\Delta x_{n,j}} \right], \tag{31}$$

where $\ell_{n,j}$ is the length of the j^{th} edge, which is an arc on the unit sphere, $\Psi_{g,n} = \Psi_g(\mathbf{\Omega}_n)$ is the angular flux along node n, $\Psi_{g,m_{n,j}}$ is the angular flux of the node $m_{n,j}$ that share the edge j with the node n and $\Delta x_{n,j}$ is the length of the arc between the two nodes n and m. Let introduce a

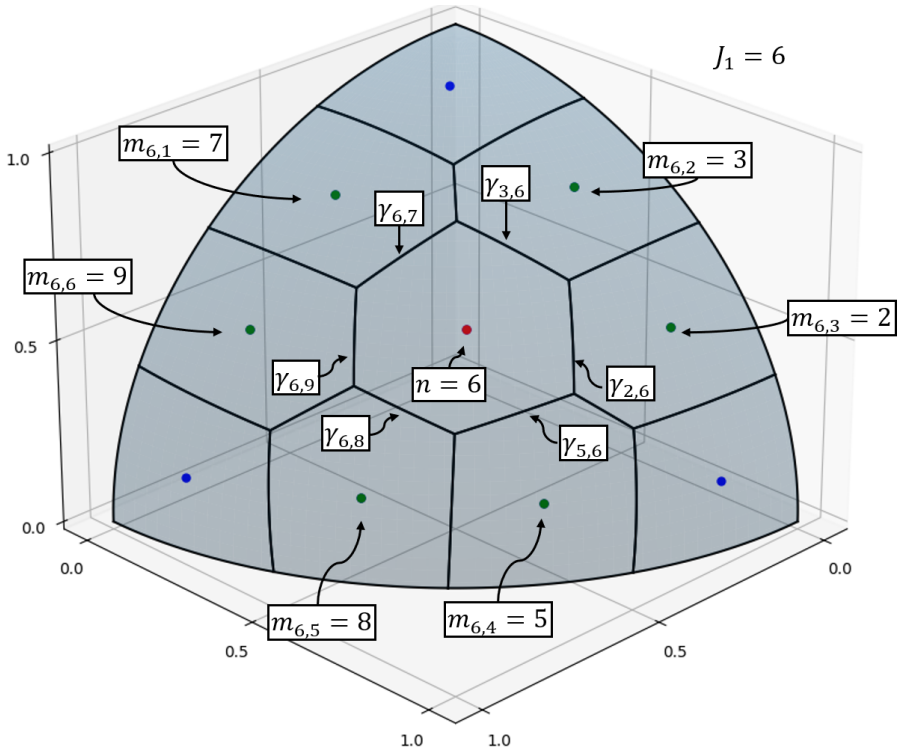

Fig. 3. Voronoi tessellation of the S_8 Carlson's level-symmetric quadrature nodes on the positive octant of the unit sphere. The red point corresponds to the node $n = 6$ and the green ones correspond to the nodes that share one of the $J_1 = 6$ edges of the region formed by the 6^{th} node.

general parameter $\gamma_{n,m_{n,j}}$, which includes both $\ell_{n,j}$ and $\Delta x_{n,j}$, that is associated with the shared edge between the nodes n. This parameter will be used as an adjustment parameter to enforce moment preservation and will differ from the ratio of $\ell_{n,j}$ and $\Delta x_{n,j}$ it substitutes. The property $\gamma_{n,m} = \gamma_{m,n}$ is enforced, such as each edge is associated with a unique coefficient $\gamma_{n,m}$ with $n < m$. The discretized AFP operator takes the form

$$Q_{g,n}^{\texttt{AFP}} = \frac{T_g}{\omega_n} \sum_{j=1}^{J_n} \gamma_{n,m_{n,j}} \left[\Psi_{g,m_{n,j}} - \Psi_{g,n} \right] . \tag{32}$$

Fig. 3 shows an example of how these relations are defined between adjacent regions on the unit sphere. A Voronoi tessellation, based on the set of quadrature nodes, is constructed over the unit sphere such as an arbitrary point on $\mathbb{S}^2$ belongs to the closest node $\mathbf{\Omega}_n$. The resulting grid is used to establish which regions share which edge. Voronoi grids for product, level-quadrature and Lebedev quadrature are shown in Fig. 1.

The values of the $\gamma_{n,m}$ coefficients will be fixed to enforce the preservation of the zeroth and first moments of the flux. Note that, regardless of the value of $\gamma_{n,m}$ values, the discretized AFP operator preserves the null space, which means that any isotropic angular flux leads to zero. Following that the spherical harmonics are eigenfunctions of the Laplace operator [10], i.e.,

$$\nabla^2_\Omega R^{m_p}_{\ell_p}(\mathbf{\Omega}) = -\ell_p(\ell_p+1) R^{m_p}_{\ell_p}(\mathbf{\Omega})\,, \tag{33}$$

the preservation of the spherical harmonics moments of the AFP operator requires the enforcement of

$$\int_{\mathbb{S}^2} d^2\Omega R^{m_p}_{\ell_p}(\mathbf{\Omega}) Q^{\texttt{AFP}}_g(\mathbf{\Omega}) = -T_g \ell_p(\ell_p+1) \int_{\mathbb{S}^2} d^2\Omega R^{m_p}_{\ell_p}(\mathbf{\Omega}) \Psi_g(\mathbf{\Omega})\,. \tag{34}$$

The zeroth and the three first moments of the AFP operator are therefore given by

$$\int_{\mathbb{S}^2} d^2\Omega Q^{\texttt{AFP}}_g(\mathbf{\Omega}) = 0 \quad \text{and} \quad \int_{\mathbb{S}^2} d^2\Omega \mathbf{\Omega} Q^{\texttt{AFP}}_g(\mathbf{\Omega}) = -2T_g \int_{\mathbb{S}^2} d^2\Omega \mathbf{\Omega} \Psi_g(\mathbf{\Omega}) \tag{35}$$

and should be preserved by the discretized AFP operator, such as

$$\sum_{n=1}^{N_d} \omega_n Q^{\texttt{AFP}}_{g,n} = 0 \quad \text{and} \quad \sum_{n=1}^{N_d} \omega_n \mathbf{\Omega}_n Q^{\texttt{AFP}}_{g,n} = -2T_g \sum_{n=1}^{N_d} \omega_n \mathbf{\Omega}_n \Psi_{g,n}\,, \tag{36}$$

with $\mathbf{\Omega}_n = (\mu_n, \eta_n, \xi_n)$. The finite-difference scheme given by Eq. 32 preserves the zeroth moment of the AFP operator for any value of $\gamma_{n,m}$. To find the parameters $\gamma_{n,m}$ that preserve the three discretized first moments of the flux, the methodology proposed by Morel *et al.* [10] is used. Explicit equations for $\gamma_{n,m}$ are obtained by defining the following complete basis

$$\mathbf{\Psi}_{g,k} = (\delta_{1,k}, \delta_{2,k}, ..., \delta_{N_d,k}) \tag{37}$$

where $\delta_{n,k}$ is the Kronecker delta. Substituting it and Eq. 32 in the rightmost expression in Eqs. 36 for each $k = 1, N_d$, one obtain N_d equations of the form

$$\sum_{j=1}^{J_k} \gamma_{k,m_{k,j}} \left[\mathbf{\Omega}_{m_{k,j}} - \mathbf{\Omega}_k\right] = -4\omega_k \mathbf{\Omega}_k\,, \tag{38}$$

where $\mathbf{\Omega}_{m_{k,j}}$ is the coordinates of the node that share the edge j with node k, for a total of $3N_d$

equations. Regardless of the choice of quadrature, it leads to an overdetermined linear system of equations since the number of unknown parameters $\gamma_{n,m}$ with $n < m$, which is equal to the total number of edges between nodes $N_{\texttt{edges}}$, is smaller than the total number of equations, $3N_d$. This can be deduced from Euler's polyhedron formula, which state that the sum of vertices $N_{\texttt{vertices}}$, edges $N_{\texttt{edges}}$ and faces N_d in a convex polyhedron, as the one formed by the quadrature nodes, is given by Euler characteristic $\chi = 2$ and from the fact that there are at least 3 edges connecting at each vertex such as $2N_{\texttt{edges}} \geq 3N_{\texttt{vertices}}$ [35]. It follows that

$$N_{\texttt{edges}} = N_d + N_{\texttt{vertices}} - 2 \leq 3N_d - 6 \leq 3N_d \,. \tag{39}$$

Fortunately, with any quadrature set we have tested, ranging from product, level-symmetric and Lebedev quadrature, the resulting system contains redundant equations, likely due to symmetry in these quadrature sets. Solving this system using the Moore-Penrose inverse [36, 37], also called pseudoinverse, gives an exact solution for $\gamma_{n,m}$ such that all the $3N_d$ equations are simultaneously satisfied. Since the system's matrix has a full column rank, the solution is unique. It is observed that all values of $\gamma_{n,m}$ are positive and respect the quadrature set symmetries. These observations will require further investigations, to assert the properties of quadrature (e.g. required symmetries) compatible with our approach, i.e. leading to an exact solution rather than an inexact least squares solution, which is usually expected with the pseudoinverse.

Using the calculated zeroth and first moment-preserving coefficients $\gamma_{n,m}$, the resulting mapping matrix is given by

$$\mathcal{M}_{n,m} = \begin{cases} -\dfrac{1}{\omega_n} \displaystyle\sum_{j=1}^{J_n} \gamma_{n,m_{n,j}} & \text{if } n = m \\ \dfrac{\gamma_{n,m}}{\omega_n} & \text{if } m \in \{m_{n,j} : j = 1, J_n\} \\ 0 & \text{otherwise} \end{cases} \tag{40}$$

The produced matrix is negative semidefinite and monotone. The presented methodology, applied to product quadrature with Chebychev azimuthal quadrature, reproduces the mapping matrix of the scheme from Morel *et al.* [10], given in Appendix A.

V. RESULTS

The benchmarks are based on pure electron transport in a water slab exposed by an infinitely wide, normally incident 10 MeV electron beam, unless noted otherwise. The energy domain is divided logarithmically into 40 energy groups, where the midpoint of the highest energy group is 10 MeV, and the cutoff energy is 1 keV. Linear discontinuous schemes are used to deal with both space and energy derivatives. Convergence criterion of 10^{-5} is used. Void boundary conditions are applied to the geometry boundaries.

Cross-sections and stopping powers for elastic, impact ionization and bremsstrahlung interactions are given by models described in Bienvenue *et al.* [16]. The elastic cross-sections are given by screened Mott cross-sections, based on the mixed uses of the unscreened Mott tabulation of Boschini *et al.* [38] and Rutherford formula with Molière screening [15], with additional low-energy and low-Z corrections from Seltzer [39] and Kawrakow [40]. This elastic model becomes highly forward-peaked as the particle energy increases, providing an interesting study case for the presented angular discretization models. The impact ionization catastrophic cross-sections are given by a modified Møller cross-sections taking into account binding energies [41, 42] over the catastrophic domain. The soft collisional stopping powers are given by subtracting the stopping powers associated with the catastrophic collisional cross-sections to the Bethe formula with density and shell corrections [43]. Finally, the bremsstrahlung catastrophic cross-sections and soft stopping powers are obtained similarly using the tabulation of Seltzer and Berger [44]. The calculation of the energy deposition cross-section in each energy group includes the addition of energy lost by the incoming electron (impact ionization and bremsstrahlung), by soft and catastrophic events, and the subtraction of the energy gain by secondary particles (the knock-on electron and the bremsstrahlung photon). The methodology to compute the total energy deposition, which consists of the energy deposited in each group and at the cutoff energy, can be found in Morel *et al.* [45] or Bienvenue *et al.* [16].

V.A. Comparison of Galerkin quadrature methods

In a conference paper [24], Morel *et al.* compared two Galerkin quadratures methods for a product quadrature defined over the unit sphere, which consist of inverting either the discrete-to-moment (**D**) or the moment-to-discrete (**M**), as presented in Sect. III. Their results show that

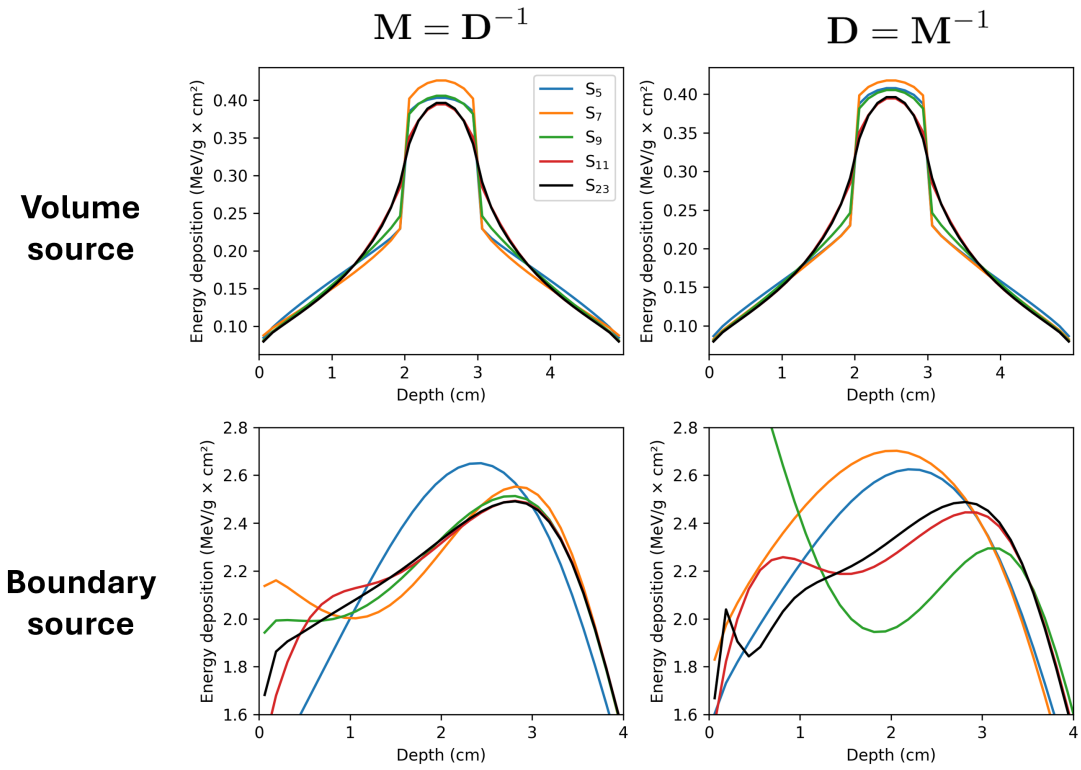

Fig. 4. Comparison of two Galerkin quadrature methods for different quadrature order for benchmark with isotropic source (top) or normally incident source (bottom).

these methods give similar flux solutions, for a benchmark in which an isotropic boundary source is defined. Recently, Shands *et al.* propose additional comparisons of these two methods with a novel Galerkin quadrature method over similar benchmarks, giving similar conclusions [3]. However, it was observed that one method is superior in some cases with quadrature defined over the unit sphere.

The 1D Cartesian geometry is used with the Lebedev quadrature. Unlike most 1D slab geometry calculations in literature, the angular domain is not simplified from the unit sphere to the main direction cosine domain between -1 and 1. The spherical harmonics must be kept as the interpolation basis rather than the Legendre polynomials, and quadrature on the unit sphere is required, as it is done in 3D Cartesian geometry. This method aims to test angular discretization on the unit sphere without relying on costly multidimensional calculations or incurring errors introduced by such calculations, such as ray effects. The geometry domain, an infinitely wide 5 cm slab, is divided into 40 voxels. The Galerkin scheme is used for the AFP operator. The first

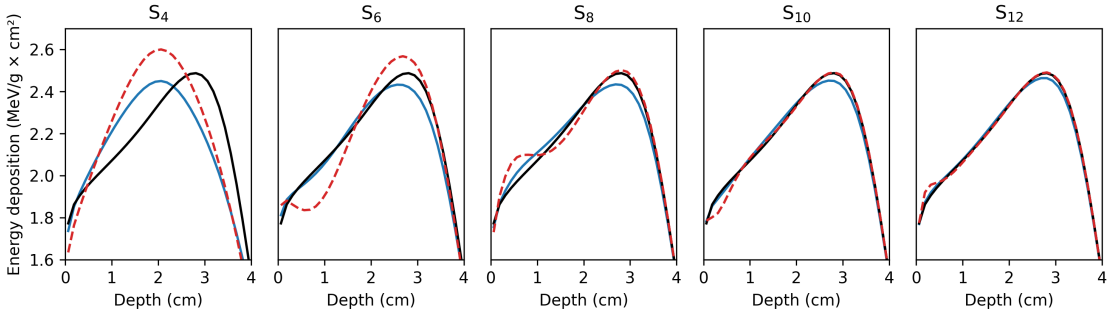

Fig. 5. Comparison of energy deposition profiles using Galerkin (in red) and finite-difference (in blue) schemes for the Fokker-Planck operator based on the Gauss-Lobatto quadrature in 1D Cartesian geometry. The reference solution (in black) is obtained using the S_{26} finite-difference scheme.

comparison consists of a benchmark with a 10 MeV isotropic source defined between 2 and 3 cm, while the second one uses a normally incident 10 MeV beam. As shown in Fig. 4, for isotropic sources, both methods give similar results for any quadrature order. This is coherent with the result in Morel *et al.* [24]. However, for the normally incident boundary source, the $\mathbf{D} = \mathbf{M}^{-1}$ energy deposition results are less accurate than the $\mathbf{M} = \mathbf{D}^{-1}$ ones at any quadrature order. Notably, the S_9 solution presents a huge overestimation of the deposited energy between 0 and 1 cm depth. Even at high quadrature order (S_{23}), while seemingly converging toward the $\mathbf{M} = \mathbf{D}^{-1}$ solution, the $\mathbf{D} = \mathbf{M}^{-1}$ solution still exhibits significant spurious oscillations. The $\mathbf{M} = \mathbf{D}^{-1}$ Galerkin quadrature method is therefore used for the following results.

V.B. Angular Fokker-Planck finite-difference schemes

The first benchmark compares Galerkin and Morel's 1D finite-difference discretization of the AFP term [8] in 1D Cartesian geometry using Gauss-Lobatto quadrature. The geometry domain, an infinitely wide 5 cm slab, is divided into 40 voxels. The Galerkin and finite-difference mapping

matrix of the S_6 case, provided to highlight their properties, are respectively given by

$$\mathcal{M}_6^{\mathtt{G}} = \begin{bmatrix} 0.0 & 20.2828 & -8.07237 & 4.48937 & -2.69983 & 1.0 \\ 3.57273 & 5.0 & 8.22289 & -2.67431 & 1.35425 & -0.475562 \\ -0.969902 & 5.60893 & 5.0 & 6.64575 & -1.82418 & 0.539401 \\ 0.539401 & -1.82418 & 6.64575 & 5.0 & 5.60893 & -0.969902 \\ -0.475562 & 1.35425 & -2.67431 & 8.22289 & 5.0 & 3.57273 \\ 1.0 & -2.69983 & 4.48937 & -8.07237 & 20.2828 & 0.0 \end{bmatrix} \tag{41}$$

and

$$\mathcal{M}_6^{\mathtt{FD}} = \begin{bmatrix} -8.51264 & 8.51264 & 0.0 & 0.0 & 0.0 & 0.0 \\ 1.49946 & -5.42257 & 3.92311 & 0.0 & 0.0 & 0.0 \\ 0.0 & 2.676 & -5.92681 & 3.25081 & 0.0 & 0.0 \\ 0.0 & 0.0 & 3.25081 & -5.92681 & 2.676 & 0.0 \\ 0.0 & 0.0 & 0.0 & 3.92311 & -5.42257 & 1.49946 \\ 0.0 & 0.0 & 0.0 & 0.0 & 8.51264 & -8.51264 \end{bmatrix}. \tag{42}$$

The finite-difference matrix is clearly monotone since the row's off-diagonal components are positive and the diagonal components are negative, and it is diagonally dominant since the sum of the row's off-diagonal components is equal to the absolute value of the diagonal components. These properties are not shared by the Galerkin matrix. Along each line n of the Galerkin matrix, corresponding to the incoming angular flux direction, the main scattering events are $n \to n-1$ (for $n \neq 1$) and $n \to n+1$ (for $n \neq N_d$), as in the finite-difference case, but farther away from the diagonal, the values sign oscillates. The negative sign for a non-diagonal element $m \neq n$ is not desirable since implies that the flux Ψ_n along the direction μ_n scatter such as there is a reduction along the direction μ_m, which does not make any physical sense. On the contrary, the finite-difference matrix is more physically robust, since the flux Ψ_n along the direction μ_n scatter such as the flux lost at $m = n$ is redistributed along the directions $m \neq n$.

The energy deposition solutions for quadrature order varying from 4 to 12 are shown in Fig. 5. The reference solution is obtained with the S_{26} finite-difference scheme. The solution using the Galerkin scheme presents significant non-physical oscillations, due to the discussed lack of monotonicity of the mapping matrix $\mathcal{M}$. These oscillations can be damped by increasing the

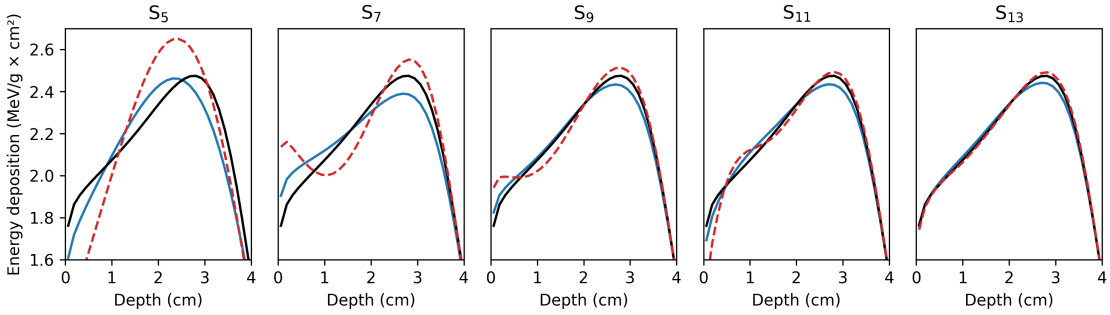

Fig. 6. Comparison of energy deposition profiles using Galerkin (in red) and finite-difference (in blue) schemes for the Fokker-Planck operator based on the Lebedev quadrature in 1D Cartesian geometry. The reference solution (in black) is obtained using the S_{23} finite-difference scheme.

quadrature order, but some artifacts can be persistent, as shown by the S_{12} case near $x = 0$ cm. This scheme used jointly with the Galerkin quadrature method, preserved N_d moments of the AFP operator [4]. It makes the Galerkin scheme a more accurate moment representation of the AFP operator than the finite-difference scheme that preserves only the zeroth and first moments. This explains the better agreement of the low-order Galerkin scheme near $x = 3$ cm with the reference solution. The finite-difference scheme is more robust for any quadrature order since it eliminates the spurious oscillations in the solution. As the quadrature order increases, both the Galerkin and finite-difference schemes tend toward the same solution.

The second benchmark compares Galerkin and the multidimensional finite-difference discretization of the AFP term in 1D Cartesian geometry using Lebedev quadrature. The geometry domain, an infinitely wide 5 cm slab, is divided into 40 voxels. The energy deposition solutions for quadrature order varying from 5 to 13 are shown in Fig. 6. The solution using the Galerkin scheme exhibits oscillations, similar than the one with the Gauss-Lobatto, but at different locations. It shows that such behavior is difficult to predict for a given quadrature choice. As the 1D AFP finite-difference scheme, the multidimensional AFP one provide a solution free of such oscillations, at the cost of the enforcement of high-order spherical harmonics moments of the AFP operator.

The third benchmark compares the Galerkin and the multidimensional finite-difference discretization of the AFP term in 3D Cartesian geometry using the Lebedev quadrature. The Cartesian geometry domain, whose size is $5 \times 5 \times 1.5$ cm along each axis, is divided into 20, 20 and 6 voxels. The source of electrons is defined over all the surface y-z at $x = 0$ and produce particle in direction $\mu = 1$. The Galerkin and finite-difference mapping matrix have respectively the same

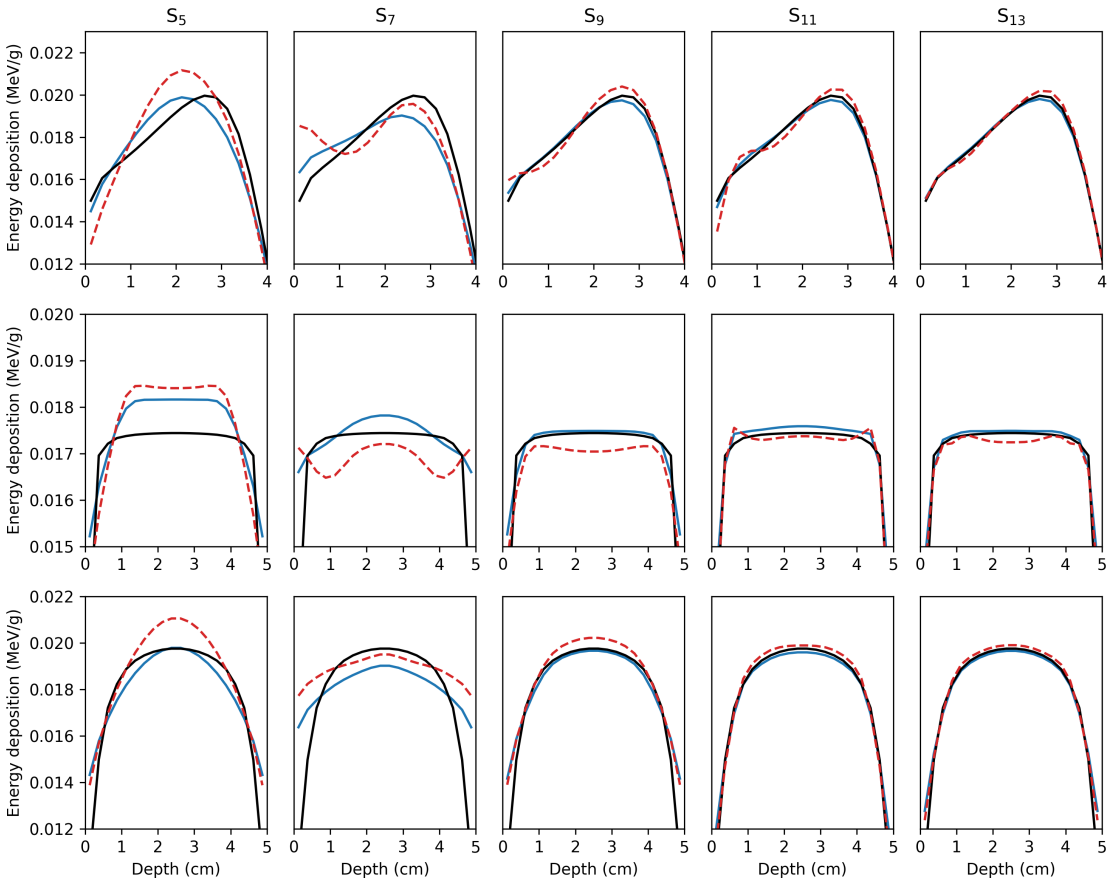

Fig. 7. Comparison of energy deposition profiles along A) $y = 2.5$ cm, B) $x = 1.25$ cm and C) $x = 2.5$ cm using Galerkin (in red) and finite-difference (in blue) schemes for the Fokker-Planck operator based on the Lebedev quadrature in 3D Cartesian geometry. The reference solution (in black) is obtained using the S_{19} finite-difference scheme.

properties as in the 1D case. The energy deposition solution for quadrature order varying from 5 to 13 is shown in Fig. 7. The solution using the Galerkin scheme presents, as expected, non-physical oscillation along both x and y spatial axis. As in the 1D case, increasing the quadrature order improves the overall monotonicity, but does not solve it. The finite-difference method, which preserves the zeroth and the three first moments of the AFP operator, eliminates any spurious oscillations of the Galerkin scheme.

The newly developed method permits monotonicity-enforcing AFP operator treatment with optimal quadrature. This is very useful for particle transport since it diminishes greatly the number of directions required to achieve a specific angular accuracy and then improves running

times. For example, the speedup of Lebedev quadrature, for S_5, S_9 and S_{17}, compared to product quadrature, for S_4, S_8 and S_{16} are respectively $\times 2.3$, $\times 3.5$ and $\times 4.7$. Lebedev quadrature also offers a better distribution of nodes and desirable symmetries. The finite-difference schemes produce more predictable solutions than the Galerkin scheme since the oscillation intensity is difficult to evaluate before calculations.

It should be noted that this method does not address the issues related to the ray effect, which is caused by the forced fulfillment of the transport equation along the discrete set of directions only and the lack of rotational invariance of the streaming operator [46].

VI. CONCLUSION

In this work, a methodology to produce monotone schemes for the multidimensional AFP operator, compatible with nonorthogonal quadrature sets and preserving the null space, the zeroth and first moments of the analytical AFP operator, is introduced. These schemes are used to treat the forward-peaked component of the elastic scattering with the Boltzmann transport equation. Results for 1D and 3D geometries calculations show that these schemes eliminate spurious oscillation related to such scattering. Further investigations will be required to assess the properties of the quadrature set, such as rotational symmetries, compatible with the proposed approach.

APPENDIX

A. FINITE-DIFFERENCE SCHEME FOR THE MULTIDIMENSIONAL ANGULAR FOKKER-PLANCK OPERATOR

The 2D finite-difference scheme using product quadrature with Chebychev azimuthal quadrature from Morel *et al.* is given by [10]

$$\mathcal{M}_{x,y} = \begin{cases} -C_n - D_{n,i} & \text{if } n = m \text{ and } i = j \\ C_n^- & \text{if } n = m+1 \text{ and } i = j \\ C_n^+ & \text{if } n = m-1 \text{ and } i = j \\ D_{n,i}^- & \text{if } n = m \text{ and } i = j+1 \\ D_{n,i}^+ & \text{if } n = m \text{ and } i = j-1 \\ 0 & \text{otherwise} \end{cases} \tag{43}$$

with $x = i + N(n-1)$ and $y = j + N(m-1)$, where the C-term are defined by Eq. 24 and the D-terms are defined by

$$D_{n,i}^- = \frac{\gamma_n}{w\left(\omega_i - \omega_{i-1}\right)\left(1-\mu_n^2\right)} \tag{44}$$

$$D_{n,i}^+ = \frac{\gamma_n}{w\left(\omega_{i+1} - \omega_i\right)\left(1-\mu_n^2\right)} \tag{45}$$

and

$$D_{n,i} = D_{n,i}^- + D_{n,i}^+ \tag{46}$$

The weights of the Chebychev quadrature are given by

$$w = \frac{\pi}{N} \quad \text{and} \quad \omega_i = \frac{(2i-1)\pi}{2N} \tag{47}$$

while the coefficients γ_n are given by

$$\gamma_n = \frac{\pi^2}{2N\left(1-\cos\left(\frac{\pi}{N}\right)\right)}\left[2(1-\mu_n^2) + \frac{\sqrt{1-\mu_n^2}}{\omega_n}\left(C_{n+1/2}d_{n+1/2} - C_{n-1/2}d_{n-1/2}\right)\right] \tag{48}$$

with

$$d_{n+1/2} = \frac{\sqrt{1-\mu_{n+1}^2} - \sqrt{1-\mu_n^2}}{\mu_{n+1} - \mu_n} \tag{49}$$

The 3D finite-difference scheme is given by

$$\mathcal{M}_{x,y} = \begin{cases} -C_n - E_{n,i} & \text{if } n = m \text{ and } i = j \\ C_n^- & \text{if } n = m+1 \text{ and } i = j \\ C_n^+ & \text{if } n = m-1 \text{ and } i = j \\ E_{n,i}^- & \text{if } n = m \text{ and } \{i = j+1 \text{ or } (i = 1 \text{ and } j = 2N)\} \\ E_{n,i}^+ & \text{if } n = m \text{ and } \{i = j-1 \text{ or } (i = 2N \text{ and } j = 1)\} \\ 0 & \text{otherwise} \end{cases} \tag{50}$$

with $x = i + 2N(n-1)$ and $y = j + 2N(m-1)$, where the C-term are defined by Eq. 24 and the E-terms are defined by

$$E_{n,i}^- = \begin{cases} \dfrac{\gamma_n}{w\left(\omega_i - \omega_{i-1}\right)\left(1-\mu_n^2\right)} & \text{if } i \neq 1 \\ \dfrac{\gamma_n}{w\left(2\pi + \omega_1 - \omega_{2N}\right)\left(1-\mu_n^2\right)} & \text{otherwise} \end{cases} \tag{51}$$

$$E_{n,i}^+ = \begin{cases} \dfrac{\gamma_n}{w\left(\omega_{i+1} - \omega_i\right)\left(1-\mu_n^2\right)} & \text{if } i \neq 2N \\ \dfrac{\gamma_n}{w\left(2\pi + \omega_1 - \omega_{2N}\right)\left(1-\mu_n^2\right)} & \text{otherwise} \end{cases} \tag{52}$$

and

$$E_{n,i} = E_{n,i}^- + E_{n,i}^+ \tag{53}$$

ACKNOWLEDGMENTS

This work was supported by the National Sciences and Engineering Research Council (NSERC) through the Discovery Grants program (Application Ids: RGPIN-2021-03899 and RGPIN-2022-03810).

REFERENCES

[1] J. E. Morel, "A hybrid collocation-Galerkin-Sn method for solving the Boltzmann transport equation," *Nuclear Science and Engineering*, **101**, *1*, 72 (1989).

[2] S. D. Pautz and M. L. Adams, "An asymptotic study of discretized transport equations in the Fokker-Planck limit," *Nuclear science and engineering*, **140**, *1*, 51 (2002).

[3] E. W. Shands, J. E. Morel, C. D. Ahrens, and B. C. Franke, "A New Galerkin Quadrature Method Not Requiring a Matrix Inverse," *Nuclear Science and Engineering*, 1–18 (2024).

[4] Y. Azmy, E. Sartori, E. W. Larsen, and J. E. Morel, "Advances in discrete-ordinates methodology," *Nuclear computational science: A century in review*, 1–84 (2010).

[5] J. S. Warsa and A. K. Prinja, "Moment-Preserving SN Discretizations for the One-Dimensional Fokker-Planck Equation," , Los Alamos National Lab.(LANL), Los Alamos, NM (United States) (2012).

[6] K. D. Lathrop, "Ray effects in discrete ordinates equations," *Nuclear Science and Engineering*, **32**, *3*, 357 (1968).

[7] M. Landesman and J. Morel, "Angular Fokker-Planck decomposition and representation techniques," *Nuclear Science and Engineering*, **103**, *1*, 1 (1989).

[8] J. E. Morel, "An improved Fokker-Planck angular differencing scheme," *Nuclear Science and Engineering*, **89**, *2*, 131 (1985).

[9] L. A. Poveda and P. Peixoto, "On pointwise error estimates for Voronoï-based finite volume methods for the Poisson equation on the sphere," *Advances in Computational Mathematics*, **49**, *3*, 36 (2023).

[10] J. E. Morel, A. Prinja, J. M. McGhee, T. A. Wareing, and B. C. Franke, "A discretization scheme for the three-dimensional angular Fokker-Planck operator," *Nuclear science and engineering*, **156**, *2*, 154 (2007).

[11] K. Przybylski and J. Ligou, "Numerical analysis of the Boltzmann equation including Fokker-Planck terms," *Nuclear Science and Engineering*, **81**, *1*, 92 (1982).

[12] G. Pomraning, "The Fokker-Planck operator as an asymptotic limit," *Mathematical Models and Methods in Applied Sciences*, **2**, *01*, 21 (1992).

[13] J. Morel, "Fokker-Planck calculations using standard discrete ordinates transport codes," *Nuclear Science and Engineering*, **79**, *4*, 340 (1981).

[14] A. Hébert, *Applied reactor physics*, Presses inter Polytechnique (2009).

[15] L. Lorence Jr, J. Morel, and G. Valdez, "Physics guide to CEPXS: a multigroup coupled electron-photon cross-section generating code," , Sandia National Lab.(SNL-NM), Albuquerque, NM (United States) (1989).

[16] C. Bienvenue, A. Naceur, A. Hébert, and J.-F. Carrier, "Toward Highly Accurate Multigroup Coupled Photon-Electron-Positron Cross-Sections for the Boltzmann Fokker-Planck Equation," Submitted to Journal of Computational Physics (May 2024).

[17] M. S. Lazo and J. Morel, "A linear discontinuous Galerkin approximation for the continuous slowing down operator," *Nuclear Science and Engineering*, **92**, *1*, 98 (1986).

[18] C. Bienvenue and A. Hébert, "High-order diamond differencing schemes for the Boltzmann Fokker–Planck equation in 1D and 2D Cartesian geometries," *Annals of Nuclear Energy*, **171**, 109032 (2022).

[19] C. Bienvenue, A. Naceur, J.-F. Carrier, and A. Hébert, "Adaptive gradient-driven coupled linear schemes and their usefulness for charged particle transport," *International Conference on Mathematics and Computational Methods Applied to Nuclear Science and Engineering (M&C 2023)* (2023).

[20] M. Caro and J. Ligou, "Treatment of scattering anisotropy of neutrons through the Boltzmann-Fokker-Planck equation," *Nuclear Science and Engineering*, **83**, *2*, 242 (1983).

[21] J. Morel, "On the validity of the extended transport cross-section correction for low-energy electron transport," *Nuclear Science and Engineering*, **71**, *1*, 64 (1979).

[22] C. R. Drumm, W. C. Fan, L. Lorence, and J. Liscum-Powell, "An analysis of the extended-transport correction with application to electron beam transport," *Nuclear science and engineering*, **155**, *3*, 355 (2007).

[23] W. H. Reed, "Spherical harmonic solutions of the neutron transport equation from discrete ordinate codes," *Nuclear Science and Engineering*, **49**, *1*, 10 (1972).

[24] J. E. Morel, J. S. Warsa, B. C. Franke, and A. K. Prinja, "Comparison of two Galerkin quadrature methods," *Nuclear Science and Engineering*, **185**, *2*, 325 (2017).

[25] R. Sanchez and J. Ragusa, "On the construction of Galerkin angular quadratures," *Nuclear science and engineering*, **169**, *2*, 133 (2011).

[26] C. Drumm, W. Fan, A. Bielen, and J. Chenhall, "Least-squares finite-element algorithms in the SCEPTRE radiation transport code," *International Conference on Mathematics and Computational Methods Applied to Nuclear Science and Engineering (M&C 2011)* (2011).

[27] C. R. Drumm, W. C. Fan, and S. D. Pautz, "Specializations in the SCEPTRE Code for Charged-Particle Transport." , Sandia National Lab.(SNL-NM), Albuquerque, NM (United States) (2018).

[28] A. McLaren, "Optimal numerical integration on a sphere," *Mathematics of Computation*, **17**, *84*, 361 (1963).

[29] B. G. Carlson, "A method of characteristics and other improvements in solution methods for the transport equation," *Nuclear science and engineering*, **61**, *3*, 408 (1976).

[30] V. I. Lebedev, "Values of the nodes and weights of ninth to seventeenth order gauss-markov quadrature formulae invariant under the octahedron group with inversion," *USSR Computational Mathematics and Mathematical Physics*, **15**, *1*, 44 (1975).

[31] V. I. Lebedev, "Quadratures on a sphere," *USSR Computational Mathematics and Mathematical Physics*, **16**, *2*, 10 (1976).

[32] V. I. Lebedev and D. N. Laikov, "A quadrature formula for the sphere of the 131st algebraic order of accuracy," *Doklady Mathematics*, **59**, *3*, 477 (1999).

[33] A. Hennink and D. Lathouwers, "A discontinuous Galerkin method for the mono-energetic Fokker–Planck equation based on a spherical interior penalty formulation," *Journal of Computational and Applied Mathematics*, **330**, 253 (2018).

[34] G. Dziuk and C. M. Elliott, "Finite element methods for surface PDEs," *Acta Numerica*, **22**, 289 (2013).

[35] D. Zwillinger, *CRC standard mathematical tables and formulas*, chapman and hall/CRC (2018).

[36] R. Penrose, "A generalized inverse for matrices," *Mathematical proceedings of the Cambridge philosophical society*, vol. 51, 406–413, Cambridge University Press (1955).

[37] Å. Björck, *Numerical methods for least squares problems*, SIAM (2024).

[38] M. Boschini, C. Consolandi, M. Gervasi, S. Giani, D. Grandi, V. Ivanchenko, P. Nieminem, S. Pensotti, P. Rancoita, and M. Tacconi, "An expression for the Mott cross section of electrons and positrons on nuclei with Z up to 118," *Radiation Physics and Chemistry*, **90**, 39 (2013).

[39] S. M. Seltzer, "An overview of ETRAN Monte Carlo methods," *Monte Carlo transport of electrons and photons*, 153–181 (1988).

[40] I. Kawrakow, "Improved modeling of multiple scattering in the voxel Monte Carlo model," *Medical physics*, **24**, *4*, 505 (1997).

[41] S. M. Seltzer, "Cross sections for bremsstrahlung production and electron-impact ionization," *Monte Carlo transport of electrons and photons*, 81–114, Springer.

[42] S. Perkins and D. Cullen, "The Livermore electron impact ionization data base," , Lawrence Livermore National Lab.(LLNL), Livermore, CA (United States) (1989).

[43] F. Salvat and P. Andreo, "SBETHE: Stopping powers of materials for swift charged particles from the corrected Bethe formula," *Computer Physics Communications*, **287**, 108697 (2023).

[44] S. M. Seltzer and M. J. Berger, "Bremsstrahlung energy spectra from electrons with kinetic energy 1 keV–10 GeV incident on screened nuclei and orbital electrons of neutral atoms with Z= 1–100," *Atomic data and nuclear data tables*, **35**, *3*, 345 (1986).

[45] J. Morel, L. J. Lorence Jr, R. P. Kensek, J. A. Halbleib, and D. Sloan, "A hybrid multigroup/continuous-energy Monte Carlo method for solving the Boltzmann-Fokker-Planck equation," *Nuclear science and engineering*, **124**, *3*, 369 (1996).

[46] J. E. Morel, T. A. Wareing, R. B. Lowrie, and D. K. Parsons, "Analysis of ray-effect mitigation techniques," *Nuclear science and engineering*, **144**, *1*, 1 (2003).